tics Communications 89 (1992) 306–315
rth-Holland

OPTICS
COMMUNICATIONS

Full length article

Aspheric holographic elements for far IR radiation

E. Hasman, N. Davidson and A.A. Friesem
Department of Electronics, Weizmann Institute of Science, Rehovot 76100, Israel

Received 1 August 1991

A novel method for designing and recording aspheric computer generated holographic optical elements for far infrared radiation has been developed. The design method is based on analytic ray-tracing procedure that exploits the minimization of the mean-squared difference of the propagation vectors between the actual output wavefronts and the desired output wavefronts. This minimization yields a solution for the aspheric grating vector. The design method is illustrated by recording and testing aspheric reflective and transmissive off-axis focussing elements for 10.6 μm wavelength having diffraction-limited performance over a broad range of incidence angles.

ntroduction

he increasing use of monochromatic radiation in complicated optical systems that require better optical formance and certain geometrical needs has results in holographic optical elements (HOEs) becoming very active [1–3]. This is particularly true for systems operating in the far infrared (IR) radiation, say 10.6 μm. such systems, holographic elements that are based on diffractive optics have several advantages over conitional elements. They are thinner, more lightweight and can perform operations that are impossible by other ans.

here are many applications using CO_2 lasers, operating at 10.6 μm wavelength, in which the HOEs can be d [4–11]. These include laser material processing [4,5], medical surgery and infrared laser radars [6,7]. such applications, since there are no practical recording materials for far IR, the HOEs must be formed using indirect recording [4–12]. In practice, a computer generated mask, representing the grating function, irst plotted with a laser scanner, then reduced in size with optical demagnification and finally recorded as elief pattern with photolithographic techniques.

)ne of the main factors that has hindered the widespread use of diffractive elements for far IR radiation, hat HOE's have relatively large amount of aberrations [1]. In order to minimize such aberrations, it is essary to exploit optimization procedures for designing aspherical grating functions of the holographic ele- nt [10,13–19]. In this paper we present such an optimization procedure in which the design is based on lytic ray tracing that minimizes the mean-square difference of the propagation vector components between actual output wavefronts and the desired output wavefronts. The minimization yields integral equations the grating vector components that can be solved analytically in some cases [10,18,19]. We shall illustrate design and recording techniques with aspheric reflective and transmissive off-axis focussing holographic nents for a readout wavelength of 10.6 μm from the CO_2 laser. The reflective and transmissive elements formed by etching either reflective metal layers or gallium arsenide substrates. These aspheric elements have raction-limited spot sizes also for plane waves arriving from relatively large incidence angles.

2. The general optimization procedure

A HOE is generally described as a combination of local gratings that change the direction of the incident rays of light. Thus, in order to find the necessary grating function for the HOE, we found that it is advantageous to first find its grating vector. This is best done by exploiting the propagation vectors of the input and output wavefronts [19].

The normalized propagation vectors, which can be regarded as the direction cosines of the input ($\hat{K}_i$) and output ($\hat{K}_o$) rays, can be written as

$$\hat{K}_o = \frac{\lambda}{2\pi}\nabla\phi_o\,, \quad \hat{K}_i = \frac{\lambda}{2\pi}\nabla\phi_i\,, \tag{1}$$

and the grating vector K_h, as

$$K_h = \frac{\lambda}{2\pi}\nabla\phi_h = K_{x_h}\hat{x} + K_{y_h}\hat{y} = \frac{\lambda}{\Lambda_x}\hat{x} + \frac{\lambda}{\Lambda_y}\hat{y}\,, \tag{2}$$

where ∇ is the gradient operator, ϕ_i and ϕ_o are the phases of the input and output wavefronts respectively, λ is the readout wavelength, ϕ_h is the grating function of the HOE and Λ_x and Λ_y are the grating spacing in x and y directions.

Fig. 1 shows the propagation of the rays for reflective and transmissive HOEs. For the reflective element, shown in fig. 1a, the input rays change the direction according to the diffraction relation from local gratings. For the transmissive element, shown in fig. 1b, the input rays, with normalized propagation vector $\hat{K}'_i$, are first refracted by the substrate of thickness t, according to the refractive relation (Snell's law), and then are diffracted from the grating that is etched on the back surface. The refractive index of the substrate is denoted by n_1, where the outer refractive indices are n_0 and n_2; typically, $n_0 = n_2 = 1$.

For the more general transmissive HOE, the propagation of the rays takes into account both the Snell's relations as well as the diffraction relations. The Snell's relations are written as

$$n_0\hat{K}'_{x_i} = n_1\hat{K}_{x_i}\,, \tag{3}$$

$$n_0\hat{K}'_{y_i} = n_1\hat{K}_{y_i}\,, \tag{4}$$

$$\hat{K}_{z_i} = \pm\sqrt{1-\hat{K}^2_{x_i}-\hat{K}^2_{y_i}}\,. \tag{5}$$

The diffraction relations are

$$\hat{K}_{x_o} = \frac{n_1}{n_2}\hat{K}_{x_i} - \frac{1}{n_2}K_{x_h}\,, \tag{6}$$

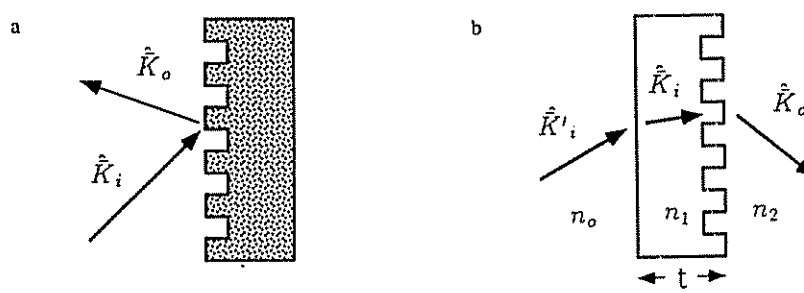

Fig. 1. The propagation of rays for HOEs. (a) Reflective HOE. (b) Transmissive HOE.

$$\hat{K}_{y_o} = \frac{n_1}{n_2}\hat{K}_{y_i} - \frac{1}{n_2}K_{y_h}, \tag{7}$$

$$\hat{K}_{z_o} = \pm\sqrt{1-\hat{K}_{x_o}^2-\hat{K}_{y_o}^2}. \tag{8}$$

Note that $\hat{K}_{x_o}^2+\hat{K}_{y_o}^2$ should be less than one, so as to avoid evanescent wavefronts. For the reflective HOE, only the diffraction relations are needed for analyzing the propagation of the rays, where $n_2=n_1=1$. As is evident from the above relations, the Snell's relations can essentially be regarded as a special case of the diffraction relations, for which $K_{x_h}=K_{y_h}=0$.

The goal when designing the grating of the HOEs is to transfer input rays into corresponding output rays that will be optimized for a given range of input parameters. The input parameters could, for example, be the direction cosine of the incoming waves, or the location of the input point sources. For a single specific input parameter it is relatively easy to form a HOE that will yield the exact desired output rays. However, for a range of input parameters, it is necessary to optimize the grating vector so as to minimize the difference between the actual and the desired output rays. The optimization is achieved by minimizing the mean-squared difference between these two sets of rays.

We shall describe the method in a two-dimensional notation. The mean-squared difference of the propagation vector components of the actual and desired output rays of the local gratings includes two scalar equations, and is written as

$$e_\perp^2(x,y) \equiv \iint [\hat{K}_{\perp d}(x,y,a,b) - \hat{K}_{\perp o}(x,y,,a,b)]^2\,da\,db, \tag{9}$$

where $\perp$ denotes the transverse vector components $\hat{x}$ and $\hat{y}$, $\hat{K}_{\perp d}(x,y,a,b)$ and $\hat{K}_{\perp o}(x,y,a,b)$ are the direction cosines of the desired and actual output rays, x and y are the space coordinates on the HOE, a and b are the input parameters for x and y coordinates, respectively.

Using the diffraction relations (eqs. (6) and (7)), differentiating $e_\perp^2(x,y)$ with respect to $K_{\perp h}(x,y)$, setting the result to zero, and noting that the second derivative of $e_\perp^2$ is always positive, yields the optimal local grating vector components,

$$K_{\perp h}(x,y) = -\iint [n_2\hat{K}_{\perp d}(x,y,a,b) - n_1\hat{K}_{\perp i}(x,y,a,b)]\,da\,db \Big/ \iint da\,db. \tag{10}$$

We now note that $e_\perp^2$ is always positive, so the minimization results for the local gratings would be identical to those for the whole HOE [19]. This implies that eq. (10) also represents the global optimal grating vector components for our desired holographic element. The optimal, two-dimensional grating function $\phi_h(x,y)$ can now be found, using eq. (2), by integrating along some arbitrary path to yield

$$\phi_h(x,y) - \phi_h(0,0) = \frac{2\pi}{\lambda}\int_c \boldsymbol{K}_h\cdot d\boldsymbol{r} = \frac{2\pi}{\lambda}\int_0^{(x,y)} K_{x_h}(x,y)\,dx + K_{y_h}(x,y)\,dy, \tag{11}$$

where $\phi_h(0,0)$ can be defined as zero.

For a unique solution, the condition of $\nabla_\perp \times \boldsymbol{K}_h = 0$ must be fulfilled, where the gradient $\nabla_\perp$ denotes $\partial\hat{x}/\partial x + \partial\hat{y}/\partial y$. This condition can be written explicitly as

$$\partial K_{x_h}(x,y)/\partial y = \partial K_{y_h}(x,y)/\partial x. \tag{12}$$

A vector that fulfills this condition is known as a conserving vector. For an on-axis holographic element, having circular symmetry, this condition is always fulfilled. An example of such an on-axis holographic element (kinoform) has been, however, developed for infrared radiation [11]. For off-axis elements, this condition is not always fulfilled, so that an exact solution for the grating function $\phi_h(x,y)$ cannot be found. Nevertheless, it is possible to obtain approximate solutions. For example, when the off-axis angle is relatively low, it is possible

to approximate the grating function by simply adding a linear phase term to the on-axis design [10,19].

Another example for which an approximate solution of $\phi_h(x, y)$ can be derived, is in some cases where $K_{x_h}(x, y)$ has weak dependence on y coordinate and $K_{y_h}(x, y)$ has weak dependence on x coordinate over the whole holographic element's area; thus, these two-dimensional grating vector components can be approximated by one-dimensional components $[K_{x_h}(x)]_{app}$ and $[K_{y_h}(y)]_{app}$. Here, the approximation is based on minimizing the mean-squared difference of the grating vector components between the optimal two-dimensional grating vector components, given by eq. (10), and the approximate one-dimensional grating vector components. The mean-squared difference for $\hat{x}$ component, for example, is defined as

$$e_x'^2(x) \equiv \int \{[K_{x_h}(x)]_{app} - K_{x_h}(x, y)\}^2 \, dy , \tag{13}$$

where $K_{x_h}(x, y)$ is given by eq. (10). Differentiating $e_x'^2(x)$ with respect to $[K_{x_h}(x)]_{app}$ and setting the result to zero, yields the approximate grating vector component

$$[K_{x_h}(x)]_{app} = \int K_{x_h}(x, y) \, dy \Big/ \int dy . \tag{14}$$

The same approximation procedure for the $\hat{y}$ component yields

$$[K_{y_h}(y)]_{app} = \int K_{y_h}(x, y) \, dx \Big/ \int dx . \tag{15}$$

Consequently, the two-dimensional grating function $\phi_h(x, y)$ can be approximated by two separated one-dimensional functions using eq. (2), and eqs. (14) and (15), to yield

$$\phi_h(x, y) \simeq \frac{2\pi}{\lambda} \int [K_{x_h}(x)]_{app} \, dx + \frac{2\pi}{\lambda} \int [K_{y_h}(y)]_{app} \, dy . \tag{16}$$

The approximation of eq. (16) is suitable for elements with relatively large f numbers.

In the general case, when the grating vector is not a conserving vector, and the above approximations are not sufficient, it is possible to find the optimal grating function by minimizing the mean-squared difference between the gradients of the optimal grating function and the optimal two-dimensional grating vector (K_{x_h}, K_{y_h}), given by eq. (10). Specifically, the function of the mean-squared difference is now given by [20]

$$e''^2(\phi_h) = \iint \left[\left(\frac{\partial \phi_h}{\partial x} - \frac{2\pi}{\lambda} K_{x_h} \right)^2 + \left(\frac{\partial \phi_h}{\partial y} - \frac{2\pi}{\lambda} K_{y_h} \right)^2 \right] dx \, dy . \tag{17}$$

Minimizing e''^2 with respect to ϕ_h can be done by using the Legendre equation, yielding the Poisson-like relation [20]

$$\nabla^2 \phi_h = (2\pi/\lambda) \operatorname{div}(K_{\perp h}) , \tag{18}$$

where $\nabla^2 = \partial^2/\partial x^2 + \partial^2/\partial y^2$ and div are the Laplacian and divergence operators, respectively. The optimal grating function may then be obtained by solving eqs. (10) and (18). Here, the procedure for solving these equations are more complicated than those for the other examples.

3. The design of a holographic focussing element

The operation and parameters of a reflective holographic focussing element (HFE) are described with the aid of the one-dimensional representation in fig. 2. Here each input plane wave converges at the output plane, to a point whose location corresponds to the angular direction of the input wave. The aperture of the HFE

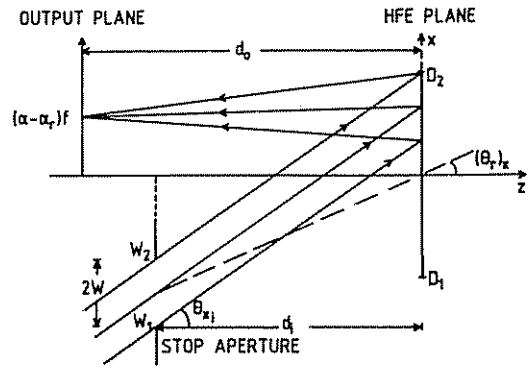

Fig. 2. The readout geometry for a reflective off-axis holographic focussing element (HFE).

extends from coordinates D_1 to D_2, whereas the width of the input stop aperture is $2W$, and it extends from coordinates W_2 to W_1. Finally, d_i and d_o are the distances from the holographic element to the input stop aperture and output plane, respectively.

We shall now describe the procedure for designing the HFE. For this design, it is convenient to let the input parameters a and b, be the direction cosines of the input plane waves

$$a=\alpha=\sin\theta_{x_i}\,, \tag{19}$$

$$b=\beta=\sin\theta_{y_i}\,, \tag{20}$$

where θ_{x_i} and θ_{y_i} are ninety degrees minus the angles between the incident ray and the x and y axes respectively. Furthermore, to simplify the presentation, we shall only deal with the $\hat{x}$ components of the propagation vectors and of the grating vector.

The normalized propagation vector of the input rays is

$$\hat{K}_{x_i}(x, y, a, b)=\alpha\,. \tag{21}$$

Now, an input plane wave, having a direction cosine α, must be transformed at a distance d_o into a spherical wave converging to a point $(\alpha-\alpha_r)f$, where $\alpha_r=\sin(\theta_r)_x$, $(\theta_r)_x$ is the off-axis angle ($(\theta_r)_y=0$), and f is a proportionality constant. Thus, the direction cosines of the desired output rays become

$$\hat{K}_{x_d}(x, y, a, b)=-\frac{x-(\alpha f-\alpha_r f)}{\sqrt{[x-(\alpha f-\alpha_r f)]^2+(y-\beta f)^2+d_o^2}}\,. \tag{22}$$

Substituting $\hat{K}_{x_i}$ from eq. (21) and $\hat{K}_{x_d}$ from eq. (22) into eq. (10), and using the approximation of eq. (14), yields

$$[K_{x_h}(x)]_{app}=-\iiint\left(\frac{-[x-(\alpha f-\alpha_r f)]}{\sqrt{[x-(\alpha f-\alpha_r f)]^2+(y-\beta f)^2+d_o^2}}-\alpha\right)\mathrm{d}\alpha\,\mathrm{d}\beta\,\mathrm{d}y\Big/\iiint\mathrm{d}\alpha\,\mathrm{d}\beta\,\mathrm{d}y\,. \tag{23}$$

To solve eq. (23), the limits of integration must be expressed by the upper $\alpha_2(x, y)$, $\beta_2(x, y)$ and lower $\alpha_1(x, y)$, $\beta_1(x, y)$ direction cosines of the input plane waves that intercept the holographic lens at a point (x, y). It is then possible to solve eq. (23) directly by numerical methods. An identical procedure is exploited for determining the $\hat{y}$ component of the grating vector $[K_{y_h}(y)]_{app.}$, and with eq. (16), the two-dimensional grating function for the reflective HFE, is found.

To evaluate the performance of the optimally designed reflective HFE, we performed a ray-tracing analysis

[21], using eqs. (6)–(8); the parameters of the reflective element were chosen as $(\theta_r)_x = 25°$, $(\theta_r)_y = 0°$, $W = 10$ mm, $f = 60$ mm, $d_0 = 60$ mm and $d_i = 54.4$ mm ($d_i = f\cos(\theta_r)_x$). The ranges of angles θ_{xi} and θ_{yi} were $20° < \theta_{xi} < 30°$ and $-5° < \theta_{yi} < 5°$ so $\Delta\theta_{xi} = \Delta\theta_{yi} = 10°$. Note that these parameters were so chosen as to enable separation between the reflected zero orders and the diffracted first order and to prevent the input stop aperture from blocking the reflected diffraction orders. We also performed a ray-tracing analysis for a HOE having a spherical grating function, given by

$$[\phi_h(x, y)]_{sph} = (2\pi/\lambda)[(x^2 + y^2 + f^2)^{1/2} + \alpha_r x] . \tag{24}$$

The geometrical parameters from the spherical HFE was the same as above, except that for this element d_i was chosen so as to optimize the focussed spot sizes, i.e., $d_i = 39$ mm.

The results of the ray tracing analysis for the two focussing elements, which do not take into account the diffraction from the aperture, are shown in fig. 3. They show the spot diagrams for the two elements as a function of nine discrete input angles of $[\theta_{xi}, \theta_{yi}]$. As shown in fig. 3a, the small central spot diagram for the spherical element is essentially ideal because the recording and readout geometries are identical. However, as the readout input angles differ from the recording angles, the spot diagrams spread substantially. Finally, as shown in fig. 3b, it is evident that the lens designed according to our optimized procedure is uniformly superior to the spherical lens, with relatively small spot diagrams, over the entire range of input angles. These results demonstrate that the spot sizes for the optimized lens, are uniformly lower than the diffraction limited size, whereas for the spherical lens, the spot sizes are much larger than the diffraction limit ($DL = 2.44\lambda f/2W \simeq 80$ μm).

We also designed a transmissive HFE by using the same procedure as for the reflective HFE, but in this case, it is necessary, first, to calculate the normalized propagation vectors of the input rays which intercept the grating, by using the refraction relations (eqs. (3), (4)). The parameters of the transmissive HFE were the same as the reflective HFE; the thickness of the element was $t = 3$ mm. The substrate of the element was gallium arsenide (GaAs), which is transparent to 10.6 μm radiation; therefore $n_1 = 3.27$ and $n_0 = n_2 = 1$. To evaluate the performance of the optimally designed transmissive HFE, we performed a ray tracing analysis, using eqs. (3)–(8). Fig. 4 shows the spot diagrams for the optimally designed transmissive HFE. The results indicate that the spot sizes for the transmissive HFE are comparable to that of the reflective HFE, i.e. diffraction limited spot sizes over the entire range of input angles.

It has been shown [17], that it is also possible to obtain diffraction limited performance by using HFE with a quadratic phase function,

$$[\phi_h(x, y)]_q = (2\pi/\lambda)[(x^2/2f_x + y^2/2f_y) + \alpha_r x] ,$$

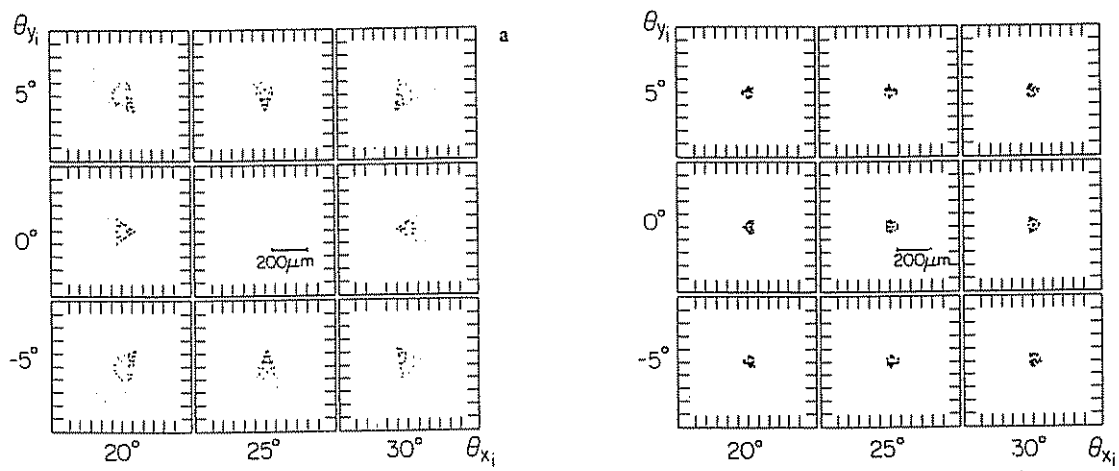

Fig. 3. Spot diagrams for the reflective HFE. (a) Spherical grating function. (b) Optimized grating function.

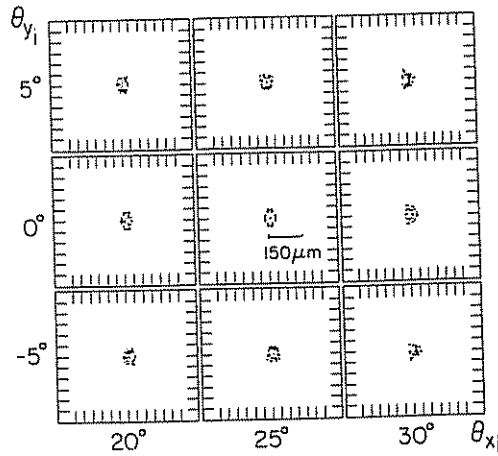

Fig. 4. The spot diagrams for the optimized transmissive HFE.

where f_x and f_y are constants. For such a function, however, f_x and f_y must be found by iterative technique (such as Code V). Furthermore, in order to ensure good optical performance for the quadratic HFE, it is necessary to optimize the geometrical parameters of the optical system, such as d_i and d_o, in fig. 2. Finally, for HFE with low f-numbers, the approximation of eq. (16) that was used in our illustrative design is no longer sufficient, and it is necessary to resort to the more complicated approach (eq. (18)) [20].

4. Experimental realization and results

In order to test our optimization procedure, we recorded reflective and transmissive HFEs. The optimized grating function was first plotted as a Lee-type [22] binary computer generated hologram (CGH) having the same parameters as those described in the preceding section. The amplitude transmittance of the CGH is given by

$$t_a = U_s\{\cos[\phi_h(x, y)]\}\,. \tag{25}$$

The term U_s is a unit step function defined by

$$\begin{aligned} U_s(\xi) &= 1\,, \quad \text{when } \xi \geqslant 0\,, \\ &= 0\,, \quad \text{when } \xi < 0\,. \end{aligned} \tag{26}$$

The binary CGH was plotted with a laser scanner (Scitex Raystar, Response 300), having resolution capabilities of about 10 μm, and recorded directly onto photographic film. The recorded plot was then demagnified optically (six times) and recorded as a chrome master mask. For realizing the reflective HFE, the information from the mask was transferred by contact printing and suitable exposure onto a glass substrate coated with aluminum and photoresist (Shipley Microposit S1400-27). After developing the photoresist, the aluminum was etched and the remaining photoresist was removed. Finally, in order to obtain a high reflective final element, a thin gold layer was vacuum deposited on the etched aluminum layer. For realizing the transmissive HFE, the information from the mask was transferred with the same photolithographic techniques as for the reflective HFE, except that for this element, the substrate was GaAs. We used a semi-insulating GaAs substrate of 3 mm thick, with a crystallographic orientation of (100) [11].

Fig. 5 shows two electron microscope pictures of a typical etched section of the modulated surface of the reflective element, each with a different magnification. As a result of the recorded and processing, we end up

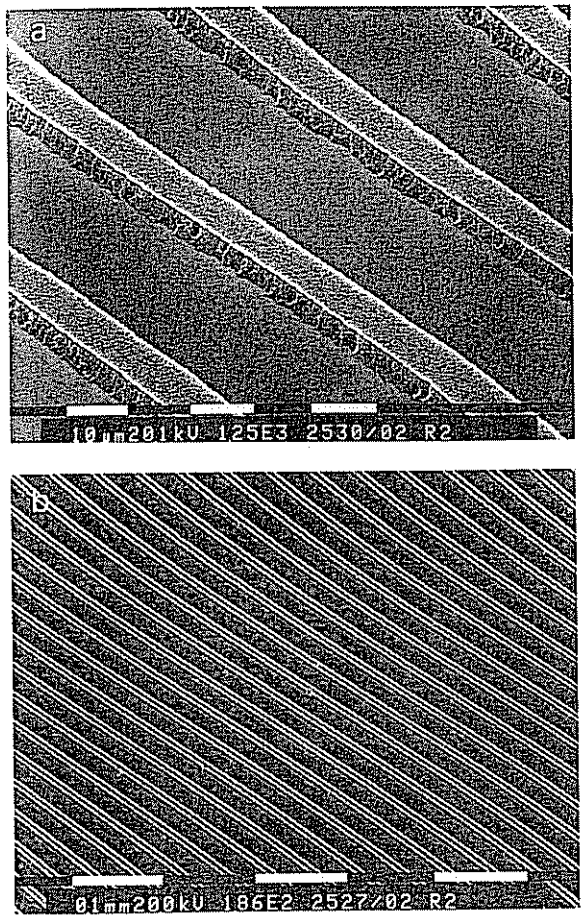

Fig. 5. Typical etched section of a modulated surface of the HFE. Each white line extends over (a) 10 μm, (b) 100 μm.

with a binary relief pattern. In the scalar approximation, an incident wavefront is multiplied by the reflectance/transmittance $H(x, y)$ of the HOE that is described by [5]

$$H(x, y) \simeq \exp\left[\mathrm{i}\left(\frac{2\pi(\Delta n)d}{\lambda} t_a(x, y)\right)\right], \tag{27}$$

where t_a is given by eq. (25), d is the depth of the surface modulation and $\Delta n = 2$ for the reflective element, while $\Delta n = n_1 - n_2$ for the transmissive element. The relevant first diffracted order is then proportional to the desired $\exp[\mathrm{i}\phi_h(x, y)]$; by setting $d \simeq \lambda/2\,\Delta n$, it is possible to maximize the diffraction efficiency to be 40.5%. Higher diffraction efficiencies, close to 100%, can be realized by using multilevel binary lithography [2,11].

The reflective and transmissive focussing elements were tested with a CO_2 laser at a wavelength of 10.6 μm. The focussed spot sizes were measured for various input plane waves by using the scanning knife-edge method [23]. Two stepper motors were used; one for moving the knife-edge and the other for changing the distance, d_{out}, from the holographic element to the measurement plane. Fig. 6 shows a representative result for the reflective element, of the relative power and relative intensity at the focussing plane, as a function of the displacement of the knife edge for an input plane wave at $\theta_{x_1} = 30°$, $\theta_{y_1} = 0°$. The relative power is depicted by the solid curve. Initially the knife edge does not block any of the focussing light so the total power is high, but as it scans across the focussed spot, it blocks more of the light. The intensity distribution at the measurement

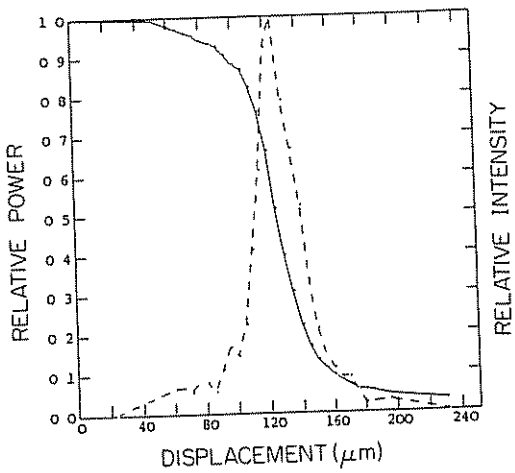

Fig. 6. Relative power of the light as a function of the displacement of the knife edge of the focussing plane for one input plane wave at $\theta_{x_1}=30°$, $\theta_{y_1}=0°$, is given by the solid curve. The corresponding intensity distribution of the focussed spot, is given by the dashed curve.

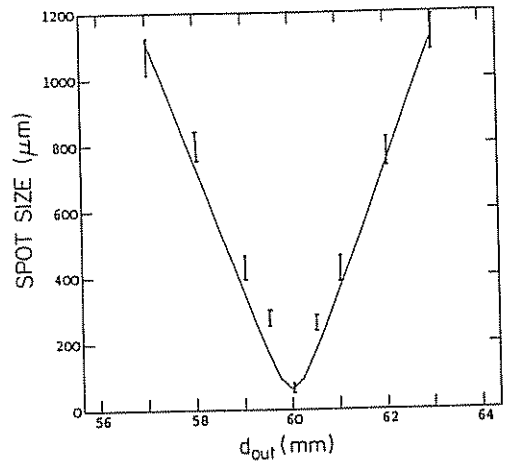

Fig. 7. The spot size as a function of the distance, d_{out}, between the hologram and the measurement plane for an input plane wave at $\theta_{x_1}=25°$, $\theta_{y_1}=0°$. The experimental data are depicted by the error bars, and the solid curve represents the calculated results.

plane was found by taking the derivative of the solid curve, and the result is shown by the dashed curve. The spot sizes were determined directly by multiplying the standard deviation of the distribution by four. The measurements were performed for the entire range of input angles, $20° < \theta_{x_1} < 30°$, $-5° < \theta_{y_1} < 5°$, and we found that the spot sizes were uniformly equal to the diffraction limit, $D_{DL} \simeq 80$ μm ($f=60$ mm, $W=10$ mm), for both reflective and transmissive HFEs.

Fig. 7 shows the spot size as a function of the distance d_{out} between the hologram and the measurement plane for one input plane wave at $\theta_{x_1}=25°$, $\theta_{y_1}=0°$, for the reflective element; the experimental data are given by the error bars. Also shown (the solid curve) are the spot sizes calculated according to the Fresnel diffraction integral [24]. For these calculations, we neglected the geometric aberrations of the focussing element. The diffraction limited spot size of 80 μm is obtained when d_{out} is 60 mm. As evident, the calculated and experimental results are in good agreement.

In the realization procedure, there are several factors that can deteriorate the spot sizes of the holographic element; the quantization of the grating function by the laser scanner, the aberrations of the optical demagnification system, and the photolithographic process. Note that for the focussing element described above, the thinnest line of the grating function, contains only four demagnified pixels of the laser scanner. Nevertheless, these factors did not significantly degrade the performance of our element, as we realized a diffraction-limited performance for the entire range of input angles.

5. Concluding remarks

In this paper, we have shown that it is possible to design and realize aspheric reflective and transmissive off-axis focussing elements, for far IR radiation, having a diffraction-limited performance over a broad range of incidence angles. The design method is based on analytic ray tracing and exploits the propagation vectors of the waves, so as to allow the realization of optimized HOEs. Results of the ray tracing analysis reveal that lenses designed according to our design method perform significantly better than spherical holographic lens. The necessary aspheric grating functions were realized by using a laser scanner and photolitographic techniques to form

a CGH. These CGH elements were tested in the laboratory, and the experimental results are in good agreement with our ray-tracing analysis; specifically, diffraction-limited spot sizes were obtained over a relatively large range of input angles.

References

[1] D.H. Close, Opt. Eng. 14 (1975) 408.
[2] G.J. Swanson and W.B. Veldkamp, Opt. Eng. 28 (1989) 605.
[3] N. Davidson, Y. Amitai, A.A. Friesem and E. Hasman, Holographic elements for coordinate transformations, SPIE 1038, Sixth meeting in Israel on optical engineering (1988) p. 162.
[4] N.C. Gallagher and D.W. Sweeney, J. Quantum Elec. 15 (1979) 1369
[5] D.K. Campbell and D.W. Sweeney, Appl. Optics 17 (1978) 3727.
[6] W.B. Veldkamp, Developments in laser-beam control with holographic diffraction gratings, SPIE 255, Practical Electro-Optical Instruments and Techniques (1980) p. 136.
[7] W.B. Veldkamp and C.J. Kastner, Appl. Optics 21 (1982) 345.
[8] D.W. Sweeney, W.H. Stevenson and N.C. Gallagher, Holography at 10.6 μm, SPIE 215, Recent Advances in Holography (1980) p. 183.
[9] G.J. Swanson and W.B. Veldkamp, Opt. Eng. 24 (1985) 791.
[10] E. Hasman, N. Davidson, A.A. Friesem, M. Nagler and R. Cohen, Meas. Sci. Technol. 1 (1990) 59.
[11] E. Hasman, N. Davidson and A.A. Freisem, Optics Lett. 16 (1991) 423.
[12] W.H. Lee, Optics Comm. 34 (1980) 29.
[13] R.C. Fairchild and R.J. Fienup, Opt. Eng. 21 (1982) 133.
[14] K.A. Winick and J.R. Fienup, J. Opt. Soc. Am. 73 (1983) 208.
[15] J. Kedmi and A.A. Friesem, J. Opt. Soc. Am. A 3 (1986) 2011.
[16] J.N. Cederquist and J.R. Fienup, J. Opt. Soc. Am. A 4 (1987) 699.
[17] J. Kedmi and A.A. Friesem, Appl. Optics 23 (1984) 4015.
[18] E. Hasman, N. Davidson and A.A. Friesem, Rev. Roum. Phys. Tome 33 N 4-6 (1988) 663.
[19] E. Hasman and A.A. Friesem, J. Opt. Soc. Am. A. 6 (1989) 62.
[20] N. Davidson, A.A. Friesem and E. Hasman, Optical coordinate transformations, Appl. Optics (1991) in press.
[21] J.N. Latta, Appl. Optics 10 (1971) 2698.
[22] W.H. Lee, Appl. Optics 13 (1974) 1677.
[23] J.A. Arnaud, W.M. Hubbard, G.D. Mandeville, B. de la Glaviére, E.A. Franke and J.M. Franke, Appl. Optics 10 (1971) 2775.
[24] M. Born and E. Wolf, Principles of optics (Pergamon Press, Oxford, 1965) ch. 8.